



Increased structural connectivity of thalamic stimulation sites to motor cortex relates to tremor suppression

Hannah H. Riskin-Jones¹, Alon Kashanian¹, Hiro Sparks, Evangelia Tsolaki, Nader Pouratian^{*}

Department of Neurosurgery, 300 UCLA Stein Plaza, Suite 562, David Geffen School of Medicine at UCLA (University of California, Los Angeles), Los Angeles, CA, United States

ARTICLE INFO

Keywords:

Deep brain stimulation
Essential tremor
Diffusion tensor imaging
Probabilistic tractography
Motor cortex
Surgical planning

ABSTRACT

Deep brain stimulation (DBS) of the ventral intermediate nucleus (VIM-DBS) is a highly successful treatment for medication-refractory essential tremor (ET). Clinical outcomes are dependent on accurate targeting. Here, we aim to develop a framework for connectivity-guided DBS targeting by evaluating probabilistic tractography and clinical response at both initial programming (IP) and clinical follow-up (CF).

Magnetic resonance imaging and clinical outcomes were evaluated in 23 ET patients who were treated by VIM-DBS at the University of California Los Angeles (20 at IP, 18 at CF, 14 at both). Lead-DBS was used to model the volume of tissue activated tissue (VTA) based on programming configurations at both IP and CF. Probabilistic tractography, calculated in FSL, was used to evaluate 1) clinically weighted whole brain connectivity of VTA; 2) connectivity between VTA and freesurfer-derived target regions of interest (ROI) including primary motor, premotor, and prefrontal cortices, and cerebellum; and 3) volume of intersection between VTA and probabilistic tractography-based segmentation of the thalamus. At IP, individual contacts were scored as high or low efficacy based on acute tremor improvement. At CF, clinical response was measured by percent of change of the Clinical Rating Scale for Tremor (CRST) compared to preoperative scores. Contributions from each target ROI to clinical response was measured using logistic regression for IP and linear regression for CF.

The clinically weighted map of whole brain connectivity of VTA shows preferential connectivity to precentral gyrus and brainstem/cerebellum. The volume of intersection between VTA and thalamic segmentation map based on probabilistic connectivity to primary motor cortex was a significant predictor of contact efficacy at IP (OR = 2.26 per 100 mm³ of overlap, $p = .04$) and percent change in CRST at CF ($\beta = 14.67$ per 100 mm³ of overlap, $p = .003$).

Targeting DBS to the area of thalamus most connected to primary motor cortex based on probabilistic tractography is associated with superior outcomes, providing a potential guide not only for lead targeting but also therapeutic programming.

1. Introduction

Essential tremor (ET) is the most common movement disorder, affecting approximately 7 million people in the United States. Of these cases, 30–50% are refractory to medications. (Louis and Ottman, 2014) ET can progress to the point of significant disability, including difficulties with employment and activities of daily living due to difficulty writing, eating, and performing fine motor movements. (Louis and Machado, 2015) Additionally, patients with ET experience social dysfunction and psychological distress, with as many as 30% of ET cases

meeting criteria for social anxiety disorder. (Lundervold et al., 2013) Deep brain stimulation (DBS) is a highly effective treatment for medication-refractory ET. However, precise DBS targeting for ET is considered crucial (Papavassiliou et al., 2004) since a relatively wide range of clinical efficacy has been observed across studies, which is likely at least in part due to differences in targeting and final lead position.

Commonly used targets include ventral intermediate nucleus (VIM), the subthalamic nucleus, the dentatorubrothalamic tract (DRTT), and the posterior subthalamic area, which encompasses the caudal zona

^{*} Corresponding author at: Department of Neurosurgery, 300 Stein Plaza, Suite 526, Los Angeles, California 90095, United States.

E-mail address: nader.pouratian@utsouthwestern.edu (N. Pouratian).

¹ Joint first authorship.

incerta (CZI). (Middlebrooks, 2020; Meng, 2013; Blomstedt, 2011) Despite being the most commonly used target, the VIM is not well visualized on standard clinical magnetic resonance imaging (MRI). (Anthofer, 2014) Consequently, the gold standard for preoperative targeting of the VIM relies on indirect localization strategies, with inferences based on visible adjacent landmarks based on atlas-derived coordinates relative to the anterior and posterior commissures, rather than visualization of nucleus itself. (Abosch et al., 2010) Thus, in most cases, patients are awoken during surgery to enable intraoperative electrophysiologic mapping and test stimulation. As this is uncomfortable for patients there is mounting interest in the field for performing DBS under general anesthesia for ET (Chen, 2018). Optimization of VIM targeting could enable lead implantation in anesthetized patients and reduce the need for intraoperative lead adjustments. Furthermore, improving stereotactic targeting of VIM would be critical to lesion-based therapies, such as MRI guided focused ultrasound and radiosurgical thalamotomy.

The pathophysiology of ET is intimately related to pathology within motor control networks, with key contributions from thalamocortical and cerebellothalamic connections. (Sharifi et al., 2014) However, the relative cortical contributions from primary motor, premotor, supplementary motor areas (SMA) are not well defined. Using white matter tractography, prior studies have identified multiple putative thalamic DBS targeting schemes, based on connectivity with primary motor, supplementary motor area and premotor cortex (Middlebrooks, 2018; Pouratian, 2011), dentate nucleus (Akram, 2018), and DRTT (Fenoy and Schiess, 2017). Indeed, in some centers, the use of DTI-based targeting has become standard practice. In the context of mixed findings and varying methodology, there is not yet consensus over the ideal connectivity-based approach. (Gravbrot et al., 2020) While there are many methods for computing tractography, probabilistic and deterministic approaches are the most common, with probabilistic tractography providing the unique benefit of analyzing quantitative voxel-wise connectivity between areas and across the brain. While the tractography methodology is an important question, here we focus on better defining the spatial patterns of connectivity associated with superior tremor control outcomes. In this study we aim to develop a framework for connectivity-guided DBS targeting and therapeutic DBS programming of the VIM using a retrospective yet integrated analysis of imaging and clinical outcomes data from both acute post-surgical testing and clinical follow-up. Analyzing the predictive durability of probabilistic tractography for DBS targeting and therapeutic programming at two distinct time-points is a unique strength of this study. We hypothesize that the efficacy of a DBS contact and the degree of clinical improvement at follow-up testing are predictable based on patterns of structural connectivity, particularly to primary motor cortex and the cerebellum.

2. Methods

2.1. Patients

Patients are drawn from neurosurgical DBS clinical database. Clinical inclusion criteria include a diagnosis of ET (Deuschl et al., 1998) (based on independent assessment of a movement disorders neurologist), having undergone DBS surgery with the VIM as target, having a clinic visit note with documentation of either initial programming data or at least four-month follow-up with tremor evaluation. Additionally, subjects were required to have the following imaging studies available: a pre-operative high resolution T1 MRI and DTI scan, and a post-operative 3D CT scan. There were 37 subjects with ET who underwent DBS implantation of the VIM at UCLA between 2014 and 2018, of which 20 met inclusion criteria for the initial programming analysis (IP) and 18 met criteria for the clinical follow-up analysis (CF), with 14 patients overlapping.

2.2. Clinical assessment

At initial programming, monopolar contacts are interrogated sequentially at progressive voltages until either maximal tremor response or prohibitive side effects are observed. Clinically observed tremor response is recorded at every voltage. Testing of each subsequent contact was only initiated after sufficient time had passed to observe spontaneous recurrence of tremor after termination of stimulation at the prior contact. Independent of imaging analysis, the response to the highest amplitude high frequency stimulation at each DBS contact (Medtronic lead model 3387) was scored on a scale from 0 to 3 corresponding to no improvement, mild, moderate, and significant improvement, respectively, based on review of the charts from initial programming only. These scores were then categorized into high (2 and 3) and low (0 and 1) efficacy groups to increase the sample size in each group and the reliability of the scoring. For the follow-up clinical response scores, we used the Clinical Rating Scale for Tremor (CRST¹⁸) to assess hand tremor severity before and after surgery. Tremor scores ranged from 0 to 32 and were derived from Part A of the CRST (three items: resting, postural, and action or intention components of hand tremor), and Part B of the CRST (five tasks comprising handwriting, drawing, and pouring) in the hand contralateral to the site of brain stimulation. We acquired post-operative tremor scores and corresponding programming parameters at least 4 months post-operatively.

2.3. Image acquisition

Each subject underwent 3 T magnetic resonance imaging on a Siemens Skyra, Prisma, or Trio scanner, including high resolution T1-weighted anatomical images using the MP-RAGE sequence [TE = 2.44 or 2.98 ms, TR = 2.1 or 2.5 s, matrix = 256 × 256, isotropic 1 mm voxels, and flip angle = 9 or 15°] and single shot spin echo planar imaging for diffusion tensor imaging [TE = 66, 72, 74, 75, or 91 ms, TR = 7, 7.1, 7.2, or 7.6 s, matrix = 128 × 128, voxel size = 1.7 × 1.7 mm or 2 × 2 mm, slice thickness = 2 or 3 mm, b-value = 1000, and 64 directions], and post-operative CT scanning with a 1 mm 3D CT, all collected as routine neurosurgical care. Variability in image parameters is due to changes in clinical scan protocol during the study period, but supports the robustness of the findings with respect to thalamocortical connectivity.

2.4. Regions of interest

The SimBio/Fieldtrip model (Horn, 2017) in Lead DBS v2.1 (Horn and Kühn, 2015) (www.lead-dbs.org) was used to calculate the volume of tissue activated (VTA) for each programming configuration. The VTAs were calculated using post-operative CT scans in native patient space (Fig. 1A). The VTAs for IP were based on sequential monopolar interrogation. For each contact, increasing voltages were tested for tremor response and side effects. A VTA was created for each contact based on the minimum voltage necessary to generate the best possible tremor response for that contact. For example, if testing at 1, 2, and 3 V all achieved moderate improvement, the VTA was specified at 1 V. As lead DBS resamples the images and VTAs to a higher resolution for modeling, the post-op CT scans and VTAs were resampled and coregistered back to raw T1 space using SPM version 12 (Friston, 1995), then registered to DTI space using the FLIRT tool in FMRIB Software Library (FSL) (Jenkinson et al., 2002; Jenkinson and Smith, 2001). Cortical regions were delineated automatically on structural MRI in Freesurfer (version 5.3.0, <http://surfer.nmr.mgh.harvard.edu/>) (Dale et al., 1999; Fischl et al., 1999). The primary motor and premotor cortex ROIs were derived from labels for Brodmann's Areas 4 and 6, respectively. (Fischl et al., 2008) The prefrontal cortex (PFC) mask was created by combining labels from the Desikan-Killiany Atlas (Desikan et al., 2006) for anterior cingulate, superior frontal, rostral and caudal middle frontal, medial orbital frontal, parsopercularis, parsorbitalis, parstriangularis, and

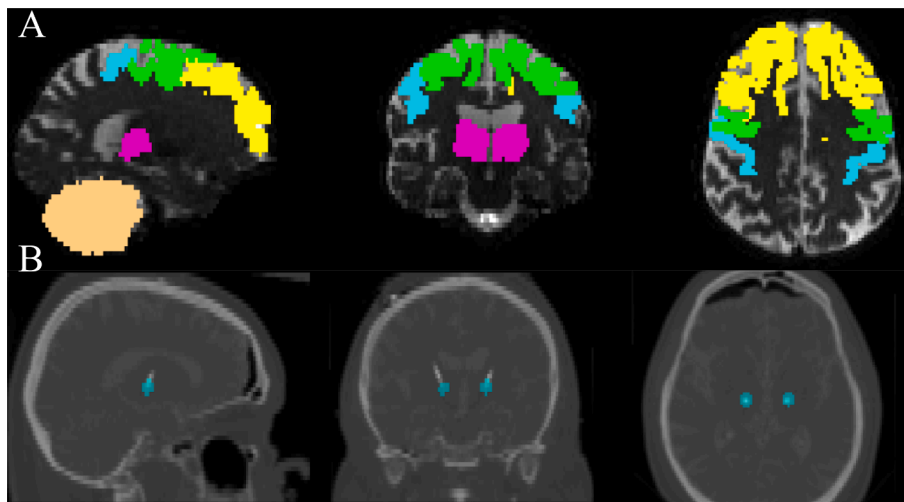


Fig. 1. Visualization of masks used for probabilistic tractography analysis. A) Target ROIs: yellow – prefrontal cortex ; green – premotor; blue – motor; pink – thalamus; brown – cerebellum B) Volume of activated tissues (VATs) (blue) overlaid on postoperative CT and DTI all co-registered in DTI space. (For interpretation of the references to colour in this figure legend, the reader is referred to the web version of this article.)

frontal pole areas (Fig. 1B). Masks for the thalamus and cerebellum were similarly derived. The ipsilateral cerebellum was used as a proxy for anatomically correct contralateral cerebellum due to technical difficulties identifying decussating fibers on tractography without using additional inclusion/exclusion masks which may bias the probability of connectivity calculation. The T1 weighted structural MRI was registered to DTI space using linear registration in FLIRT (Jenkinson et al., 2002; Jenkinson and Smith, 2001). ROIs were then registered to DTI space according to the same transformation matrix.

2.5. Tractography analysis

Probabilistic diffusion tractography was performed to define structural connectivity of the VTAs and thalamus with target ROIs (for both IP and CF timepoints) using the FMRIB's Diffusion toolbox. Eddy currents and subject motion were corrected by registering each volume in the diffusion dataset to the initial reference B0 volume with an affine transformation. Skull stripping was performed using the brain extraction tool (BET) (Smith, 2002). Diffusion tensors were fit to the data then BEDPOSTX was used to build distributions around each tensor (Behrens et al., 2007; Behrens, 2003). This model uses Bayesian techniques to estimate a probability distribution function (PDF) on the principal fiber direction at each voxel, accounting for the possibility of crossing fibers. Two fibers were modeled per voxel, with a multiplicative factor of 1 for the prior on the additional modeled fibers, and 1000 iterations performed before sampling (Behrens et al., 2007). Using these PDFs and PROBTRACKX, we then determined the probability of connectivity between seed and the ROI targets. From each voxel in the seed, 5000 streamlines were generated; a 0.2 curvature threshold was chosen, and a loop check termination was used.

When tracking from VTAs, the target masks were used as classification masks. The probability of VTAs connectivity to each target ROI was then calculated by dividing the number of streamlines connecting the VTA to the target ROI by the total number of streamlines sent out (5000 streamlines per seed voxel) (Tsolaki et al., 2021).

When tracking from thalamus, the target masks were used as way-point masks. The resulted 'thalamic probability maps' identified the regions within thalamus with the highest probability of connectivity with the ROIs. Thresholds were applied to these maps in order to define an area of the thalamus most connected to each ROI ('probabilistic thalamic target'; PTT). Thresholds were based on the maximum intensity value of the segmented thalamic maps. The ideal threshold is unknown, so thresholds of 30, 40 and 50% were applied as has been

described previously. (Tsolaki et al., 2018) At each threshold, the volume of overlap was calculated between each VTA and the PTT for each ROI.

2.6. Efficacy maps

We used a similar approach as we have previously published. (Andersson et al., 2010) Using the same tractography parameters described above, VTA for each contact (at IP) and the final programming configuration (at CF) were used as seeds to perform whole brain tractography. The resulting whole brain maps were registered nonlinearly using FNIRT (Park et al., 2004) in to MNI (152 2 mm) space. Then, each individual tractography result was binarized at a 0.02 threshold. A common population map in MNI space was created by summing tractography results over all contacts and subjects, then a threshold was applied to include only voxels that were present in at least 20% of contacts. To create the 'contact efficacy map,' the individual binarized tract maps were first weighted by the tremor response score of that contact. Then the average map across all subjects was calculated to create the 'average contact efficacy map,' with each voxel's value in the map corresponding to the average tremor response score of the contacts with connectivity to that specific voxel. To make the 'clinical efficacy map', the individual results were weighted by the clinical response, measured by percent change in CRST, for each hemisphere. These maps were then averaged to create an 'average clinical efficacy map,' with each voxel's value in the map corresponding to the average clinical response of the patients with connectivity to that specific voxel. Both maps were then restricted to their respective common population map to reduce noise.

2.7. Statistical analysis

Statistical analysis was conducted in SPSS v. 26 and R. A significance level of ≤ 0.05 was used for all tests. *Probability of connectivity:* For IP, a logistic regression was calculated using the probabilities of connectivity to each target ROI as independent variables and the contact efficacy group (high vs. low) as the binary dependent variable. For CF, a linear regression was calculated using the probability of connectivity to each target ROI as independent variables and the percent change in CRST after surgery as the continuous dependent variable. Betas are presented per 100 mm³ of overlap for ease of interpretation. *Volume of Intersection:* We assessed the relationship between volume of overlap of VTA and the PTT for each ROI and 1) contact efficacy group (high vs. low) at IP; 2)

percentage of clinical improvement at CF. For the IP timepoint, a logistic regression was used with the dependent variable contact efficacy and the independent variables the volume overlap. For the CF time point a linear regression was used with the dependent variable percent change in CRST scores at clinical follow-up and the independent variables the volume overlap. Each regression model was calculated for the 30, 40, and 50% thalamic segmentation map thresholds and betas are presented per 100 mm³ of overlap for ease of interpretation. As a post-hoc analysis, we used empirical receiver operating characteristic (ROC) curves to examine the sensitivity and specificity at all possible cutoffs (Avecillas-Chasin et al., 2015) of the overlapping between our VTAs and the motor-PTT (the PTT for primary motor cortex). We report the area under the curve (AUC) and 95% confidence intervals (CI) for each threshold. For CF, clinical response scores were split at the median value to create a binary variable for the purposes of classification.

3. Results

3.1. Participants

At IP, we assessed 20 subjects, with a total of 107 contacts analyzed. At CF, there were 18 subjects with a total of 29 hemispheres analyzed. Detailed patient characteristics can be found in Table 1.

3.2. Efficacy maps

Efficacy maps were created to delineate the connectivity patterns underlying contact efficacy and clinical response. Whole brain probabilistic tractography was performed seeded from the VTAs of each individual contact and the programming configuration at the time of CF. The average clinical efficacy map for both timepoints demonstrates improved therapeutic tremor response associated with stronger structural connectivity to both the precentral gyrus and the cerebellum (Figs. 2 and 3).

3.3. Volume of intersection between VTAs and thalamic segmentation maps

We calculated the intersection between VTA and tractography-based thalamic segmentations at various probability thresholds (Supplementary Table 1). Multiple regression models were calculated for each timepoint and at each of three thresholds for the PTTs: 30, 40, and 50%

Table 1
Patient characteristics.

Patient characteristic	Mean (sd)/n
Age	66.17 (13.39)
Gender	
Female	14
Male	9
Disease Duration	32.7 (16.6)
Family History of ET	
Yes	16
No	5
Unknown ^a	2
Electrode laterality	
Left	9
Right	2
Bilateral	12
Days to initial programming	22.80 (12.69)
Days to clinical follow-up	405.22 (286.33)
Contact efficacy	2.18 (0.79)
Contact efficacy group	
High	83
Low	24
CRST pre-operative	18.80 (5.67)
CRST at clinical follow-up	6.30 (4.17)
CRST – clinical rating scale for tremor ^a 2 patients had unknown family history due to adoption	

of the maximum intensity value. At IP, the volume of overlap between VTA and the motor-PTT (using the 40% thresholds) was a significant predictor of clinical response at each contact (OR = 2.26, $p = .04$) (Table 1A). This means that for an increase of 100 mm³ (Lundervold et al., 2013) in overlap between the contact VTA and the 40% threshold motor-PTT, the odds of a high efficacy contact increased by a factor of 2.26, holding all other variables constant. Volumes of intersection for premotor, PFC, and cerebellar PTTs were not significant predictors of efficacy at IP. At the 30 and 40% thresholds, none of the predictors were significant. In linear regression analyses, greater volume of overlap between motor-PTT and VTA was a significant predictor of improvements in CRST (40%: $\beta = 10.3$, $p = .03$; 50%: $\beta = 14.67$, $p = .003$). The overall model fit was $R^2 = 0.13$ for the 40% threshold model and $R^2 = 0.24$ for the 50% threshold model (Table 1B). This means that for an increase of 100 mm³ in overlap between the contact VTA and the 40% threshold motor-PTT, the percent change in CRST is expected to increase by 10.3, holding all other variables constant. For an increase of 100 mm³ in overlap between the contact VTA and the 50% threshold motor-PTT, the percent change in CTRS is expected to increase by 14.67, holding all other variables constant. At the 30% threshold, none of the predictors were significant. Finally, volumes of intersection for premotor cortex, PFC, and cerebellum PTTs were not significant predictors.

3.4. Post-Hoc ROC analysis

Given the significance of the motor cortex in the statistical analysis, the sensitivity and specificity of this predictor was further analyzed using ROC curves. The analysis of ROC curves showed that the volume of overlap between the VTA and probabilistic tractography-based motor cortical thalamic segmentation could predict which contacts would be effective at initial programming and which patients had a superior clinical outcome at least 4 months after DBS surgery. The area under the ROC curves (AUC) at initial programming were 0.64 (CI: 0.52-0.77), 0.64 (CI: 0.52-0.76) and 0.62 (CI: 0.50-0.74) for the 30, 40, and 50% thresholds, respectively, and at clinical follow-up were 0.71 (CI: 0.52-0.91), 0.72 (CI: 0.52-0.92), and 0.73 (CI: 0.53-0.92) (Fig. 4).

3.5. Probability of connectivity to target regions

The regression models for quantitatively comparing the probability connectivity of VTAs to target ROIs for high and low efficacy contacts at initial programming and for percent change in CRST at clinical follow-up did not reveal any significant predictors (Supplementary Table 2).

4. Discussion

We aimed to identify connectivity features that predict the efficacy of individual DBS contacts, with the goal of providing a basis and rationale for a personalized method of surgical targeting and programming based on probabilistic tractography. We present a ‘contact efficacy map’ and ‘clinical efficacy map’ which illustrate the connectivity patterns of efficacious VTAs at both IP and CF, with prominent connections to both precentral gyrus and cerebellum/brainstem. We additionally found predictive value in the volume of overlap between the VTA and the motor-PTT which is an area of the thalamus that is most highly connected to the motor cortex. This finding held true both soon after surgery at initial programming and at a clinical follow up, at least four months later, which generally had more complex programming configurations. Consistency of clinical efficacy of DBS electrodes at both IP and CF timepoints, demonstrates the durability of initial results over time. Therefore, volume of overlap between VTA and primary motor-PTT, could help to guide thalamic targeting during initial lead implantation and inform subsequent programming during clinic follow up. This is the first study to identify connectivity-based predictors of DBS success at multiple timepoints.

Associations between ET clinical scores and volume of overlap

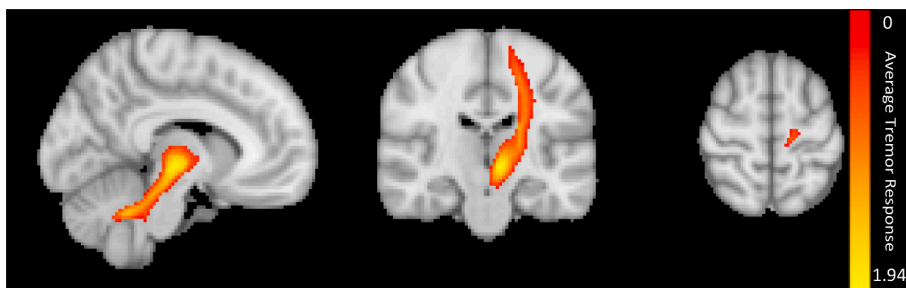


Fig. 2. Contact Efficacy Map for Initial Programming (IP). Whole brain tractography was calculated from the VAT for each contact. Each individual result was registered to MNI space, binarized at a 0.02 threshold, then weighted by the IP tremor response score. An average was taken across all subjects and contacts, then restricted to include only voxels that were present in at least 20% of contacts. Each voxel represents the average efficacy of contacts with connectivity to that voxel. Left- and Right-sided contacts have been combined into one map.

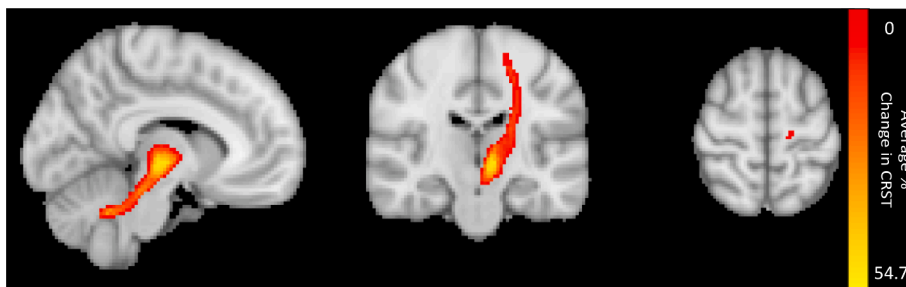


Fig. 3. Clinical Efficacy Map for Clinical Follow-up (CF). Whole brain tractography was calculated from the VAT for each programming configuration at CF (one per hemisphere). Each individual result was registered to MNI space, binarized at a 0.02 threshold, then weighted by the percent change in Clinical Response Score for Tremor (CRST). An average was taken across all subjects and hemispheres, then restricted to include only voxels that were present in at least 20% of hemispheres. Each voxel represents the average percent change in CRST of programming configurations with connectivity to that voxel. Left- and Right-sided contacts have been combined into one map.

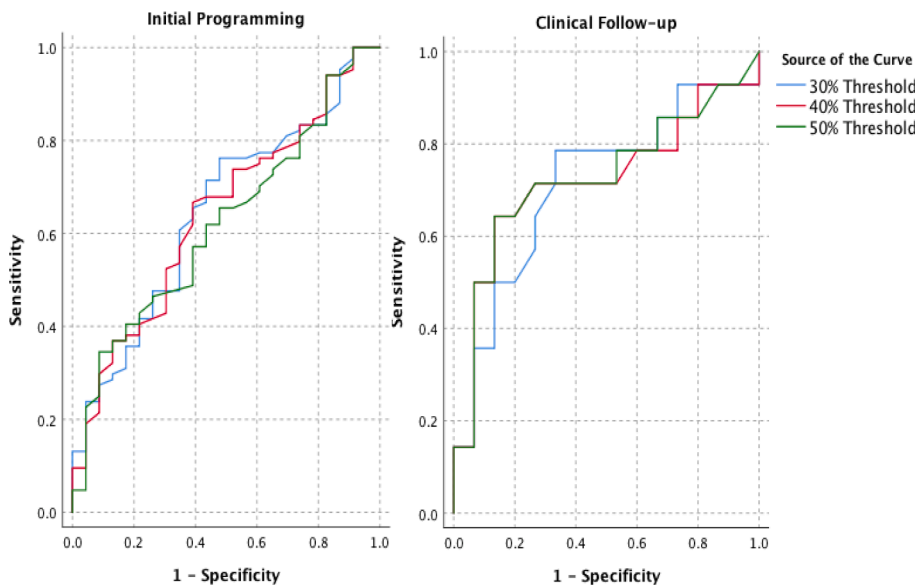


Fig. 4. ROC Curves for Motor Cortex. As a post-hoc analysis, we used empirical receiver operating characteristic (ROC) curves to examine the sensitivity and specificity at all possible cutoffs of the overlapping between the volume of activated tissue (VAT) and the probabilistic thalamic target for primary motor cortex. The area under the ROC curves (AUC) at initial programming were 0.64 (CI: 0.52-0.77), 0.64 (CI: 0.52-0.76) and 0.62 (CI: 0.50-0.74) for the 30, 40, and 50% thresholds, respectively, and at clinical follow-up were 0.71 (CI: 0.52-0.91), 0.72 (CI: 0.52-0.92), and 0.73 (CI: 0.53-0.92) (Fig. 4).

between DBS contacts and DTI targets has been identified in multiple prior studies. (Middlebrooks, 2018; Akram, 2018) However, the optimal selection of ROIs for deriving thalamic segmentation maps remains poorly defined, with inconsistencies across studies. Here we report unique clinical significance of thalamocortical connections to primary motor cortex (or precentral gyrus). Our findings are consistent with prior work by Tsolaki *et al* who found predictive value in the overlap between thalamotomy lesion and thalamic regions most highly connected to primary motor cortex. (Andersson *et al.*, 2010) On the other hand, our group previously reported greater efficacy amongst contacts most closely associated with thalamic projections to the premotor cortex, rather than primary motor cortex. (Pouratian, 2011) The methods used to define cortical targets were less precise in our prior work and VTAs and clinical efficacy were not considered previously. Still, that findings were corroborated by Middlebrooks *et al* who also reported

greater clinical improvement in patients with stimulation in thalamic areas that were highly connected to SMA and premotor cortex. (Middlebrooks, 2018) In a study of five patients with ET and four patients with PD tremor, Akram *et al*, found volume of overlap with an area of the thalamus highly connected to the contralateral dentate nucleus was the unique predictor of clinical efficacy. (Akram, 2018) In their study, the thalamic-dentate target lay within the thalamic-primary motor target, which could indicate a capacity to further optimize the present results. Although we did not directly test connectivity to contralateral dentate nucleus, the increase in beta coefficient with higher, more refined thresholds at CF suggests that VTA overlap more strongly predicts clinical efficacy with smaller, more precise motor thalamic targets. While there remains inconsistency among the specific thalamic targets, analyzing the volume of overlap appears to be a useful approach to DBS targeting.

Table 2
Regression models for volume of overlap between VTA and thalamic segmentation maps.

A. Initial Programming												
	30% Threshold				40% Threshold				50% Threshold			
	exp(β)	β (Std. Error)	z	p	exp(β)	β (Std. Error) ^a	z	p	exp(β)	β (Std. Error) ^a	z	p
Motor	2.12	0.75 (0.43)	1.75	0.08	2.26	0.81 (0.40)	2.03	0.04	2.31	0.84 (0.42)	1.98	0.05
Premotor	1.38	0.32 (0.35)	0.90	0.37	1.54	0.43 (0.31)	1.40	0.16	1.91	0.65 (0.37)	1.73	0.08
Prefrontal	0.70	-0.36 (0.47)	-0.76	0.45	0.58	-0.54 (0.43)	-1.26	0.21	0.60	-0.51 (0.51)	-1.00	0.32
Cerebellum	0.70	-0.36 (0.41)	-0.87	0.39	0.66	-0.42 (0.47)	-0.89	0.37	0.49	-0.71 (0.56)	-1.28	0.20
B. Clinical Follow-up												
	β (std. Error)	t	p	β (std. Error)	t	p	β (std. Error)	t	p	β (std. Error)	t	p
Motor	0.08 (0.04)	1.92	0.07	0.10 (0.04)	2.39	0.03	0.15 (0.05)	3.25	0.003	0.08 (0.04)	1.92	0.07
Premotor	0.04 (0.06)	0.70	0.49	0.04 (0.05)	0.83	0.42	0.05 (0.05)	1.16	0.26	0.04 (0.06)	0.70	0.49
Prefrontal	-0.02 (0.06)	-0.28	0.78	-0.01 (0.06)	-0.19	0.85	0.006 (0.06)	0.09	0.93	-0.02 (0.06)	-0.28	0.78
Cerebellum	-0.05 (0.06)	-0.82	0.42	-0.08 (0.07)	-1.14	0.27	-0.18 (0.09)	-2.07	0.05	-0.05 (0.06)	-0.82	0.42
R-squared	0.11			0.13			0.24					

A) Initial programming: results of logistic regressions with the independent variable contact efficacy and the dependent variables the volume overlap between thalamic segmentation maps based on connectivity to target ROIs with the VTAs b) clinical follow-up: results of linear regression with the dependent variable percent change in CRST scores at 6-month follow-up and the independent variables the volume overlap between thalamic segmentation maps based on connectivity to target ROIs with the VTAs. Results of the regressions are shown for the 30%, 40%, and 50% thresholds of the thalamic segmentation map. *p*-values ≤ 0.05 are in boldface. ^a β are presented per 100 mm³ of overlap.

The only connectivity based targeting method which has been tested prospectively is targeting of the DRTT, which relates the three main targets for DBS (it interconnects VIM and CZI, and passes near the STN.) Fenoy *et al* reported successful outcomes in prospective study in 20 patients with tractographic targeting of the DRTT. (Fenoy and Schiess, 2017) While DRTT-tractography yielded similar stereotactic targets to traditional indirect methods, large discrepancies were reported in two subjects who had large ventricles and/or a long distance between the anterior and posterior commissures. Furthermore, clinical utility of DRTT based mapping may be limited because its delineation requires advanced techniques and is most accurately performed with HARDI data, which is associated with extended scanning time and is not a standard part of clinical scanning protocols. (Akram, 2018) By contrast, probabilistic tractography between thalamus and motor cortex can be performed reliably using standard clinical diffusion acquisitions. While probabilistic tractography allows quantitative thresholds to be applied to thalamic segmentation maps in order to create precise connectivity based targets for DBS, it is a time consuming computational method. Deterministic tractography is an alternative method for evaluating connectivity based targets. (Petersen, 2017) Future work building on the current findings by directly comparing deterministic and probabilistic tractography methods, as has previously been in the subthalamic nucleus for Parkinson disease, (Yamada, 2010) would support and clarify the clinical utility of the motor-PTT as a robust target for DBS.

Despite significant findings, limitations are noted. First, this is a retrospective clinical study with limited sample size and multiple scanning parameters used over the course of the study period. Second, the VTA models are only approximations based on the contact location and voltage and may be affected by local factors such as tissue heterogeneity. Additionally, no distortion correction was applied to the DTI data which may have affected the localization of the VTA. Third, we were unable to successfully compute tractography to the contralateral cerebellum and have therefore used connectivity to ipsilateral cerebellum as a proxy, although it is not anatomically correct. Identification of the decussating fibers of the DRTT on diffusion tensor tractography is difficult due to limitations in depiction of crossing fibers. For this reason, many studies have similarly utilized ipsilateral regions of interest in order to construct cerebello-thalamocortical (CTC) fibers for DBS targeting purposes without needing to map decussating fibers. (Coenen *et al.*, 2014; Habas and Cabanis, 2007) Using probabilistic tractography, Habas and colleagues identified an ipsilateral DRTT, with ipsilateral projections from the dentate nucleus to the red nucleus and passing through the ipsilateral ventrolateral thalamus in five normal subjects.⁴⁰ The authors hypothesized that this ipsilateral reconstructed pathway consisted of the “true” ipsilateral pathway up to the tegmental

decussation and the contralateral pathway of the DRTT beyond this decussation. Hence, the cerebello-thalamic fibers and resultant cerebello-thalamic probabilistic segmentation map in our study were likely produced based on the combination of these two fiber pathways. We acknowledge that this may have influenced the results of our study. Fourth, there are lack of consistent methods for threshold selection when using probabilistic tractography. Our current method uses a threshold of 0.02 based on visual inspection. We submit that this is an area for improved methodology but that threshold selection likely ultimately depends on multiple factors including targets and tracts of interests as well as imaging parameters. Finally, we did not record side effects in our study. Thus, although we did identify regions associated with greatest clinical outcome, we did not take adverse effects into account.

Future work will focus on translating the connectivity features identified in this report into practical DBS programming configurations and prospectively testing this paradigm in ET patients.

5. Conclusion

Improving electrode targeting will personalize the DBS target with the aim of making electrode placement and programming more efficient, increasing battery life, and reducing tremor severity in patients. These improvements will particularly affect patients whose individual anatomy deviates the most from normal. In sum, ET is a common and disabling condition for which DBS is an effective but still evolving therapy. Developing a targeting system using imaging analysis techniques like probabilistic tractography may potentially increase efficiency and improve patient outcomes.

Funding

This work was partially supported by the AOA Carolyn L. Kuckein Student Research Fellowship. Funding sources had no active role in conducting research.

CRedit authorship contribution statement

Hannah H. Riskin-Jones: Conceptualization, Methodology, Formal analysis, Investigation, Data curation, Writing - original draft. **Alon Kashanian:** Conceptualization, Methodology, Formal analysis, Investigation, Data curation, Writing - original draft. **Hiro Sparks:** Investigation, Writing - review & editing. **Evangelia Tsolaki:** Methodology, Formal analysis, Investigation, Writing - review & editing, Supervision. **Nader Pouratian:** Conceptualization, Methodology, Resources, Writing

- review & editing, Supervision, Project administration, Funding acquisition.

Declaration of Competing Interest

The authors declare that they have no known competing financial interests or personal relationships that could have appeared to influence the work reported in this paper.

Appendix A. Supplementary data

Supplementary data to this article can be found online at <https://doi.org/10.1016/j.nicl.2021.102628>.

References

- Abosch, A., Yacoub, E., Ugurbil, K. & Harel, N. An assessment of current brain targets for deep brain stimulation surgery with susceptibility-weighted imaging at 7 tesla. *Neurosurgery* 67, 1745–1756 (2010).
- Akram, H., et al., 2018. Connectivity derived thalamic segmentation in deep brain stimulation for tremor. *NeuroImage Clin.* 18, 130–142.
- Andersson, J., Jenkinson, M. & Smith, S. (2010). Non-linear registration, aka spatial normalisation.
- Anthofer, J., et al., 2014. The variability of atlas-based targets in relation to surrounding major fibre tracts in thalamic deep brain stimulation. *Acta Neurochir. (Wien)* 156, 1497–1504.
- Avencillas-Chasin, J.M., Alonso-Frech, F., Parras, O., del Prado, N., Barcia, J.A., 2015. Assessment of a method to determine deep brain stimulation targets using deterministic tractography in a navigation system. *Neurosurg. Rev.* 38, 739–751.
- Behrens, T.E.J., et al., 2003. Characterization and Propagation of Uncertainty in Diffusion-Weighted MR Imaging. *Magn. Reson. Med.* 50, 1077–1088.
- Behrens, T.E.J., Berg, H.J., Jbabdi, S., Rushworth, M.F.S., Woolrich, M.W., 2007. Probabilistic diffusion tractography with multiple fibre orientations: What can we gain? *Neuroimage* 34, 144–155.
- Blomstedt, P., et al., 2011. Deep brain stimulation of the subthalamic nucleus versus the zona incerta in the treatment of essential tremor. *Acta Neurochir. (Wien)* 153, 2329–2335.
- Chen, T., et al., 2018. Intraoperative test stimulation versus stereotactic accuracy as a surgical end point: A comparison of essential tremor outcomes after ventral intermediate nucleus deep brain stimulation. *J. Neurosurg.* 129, 290–298.
- Coenen, V. A. et al. (2014). Modulation of the Cerebello-Thalamo-Cortical network in thalamic deep brain stimulation for tremor: A diffusion tensor imaging study. *Neurosurgery* 75, 657–669.
- Dale, A.M., Fischl, B., Sereno, M.I., 1999. Cortical surface-based analysis. I. Segmentation and surface reconstruction. *Neuroimage* 9 (2), 179–194.
- Desikan, R. S. et al. An automated labeling system for subdividing the human cerebral cortex on MRI scans into gyral based regions of interest. (2006). doi:10.1016/j.neuroimage.2006.01.021.
- Deuschl, G. et al. Consensus statement of the Movement Disorder Society on tremor. in *Movement Disorders* 13, 2–23 (Lippincott Williams and Wilkins, 1998).
- Fenoy, A.J., Schiess, M.C., 2017. Deep Brain Stimulation of the Dentato-Rubro-Thalamic Tract: Outcomes of Direct Targeting for Tremor. *Neuromodulation Technol. Neural Interface* 20, 429–436.
- Fischl, B., Sereno, M.I., Dale, A.M., 1999. Cortical surface-based analysis. II: Inflation, flattening, and a surface-based coordinate system. *Neuroimage* 9 (2), 195–207.
- Fischl, B. et al. Cortical Folding Patterns and Predicting Cytoarchitecture. *Cereb. Cortex* August 18, 1973–1980 (2008).
- Friston, K.J., et al., 1995. Spatial registration and normalization of images. *Hum. Brain Mapp.* 3, 165–189.
- Gravbrot, N., Saranathan, M., Pouratian, N., Kasoff, W., 2020. Advanced Imaging and Direct Targeting of the Motor Thalamus and Dentato-Rubro-Thalamic Tract for Tremor: A Systematic Review. *Stereotact. Funct. Neurosurg.* 98 (4), 220–240.
- Habas, C., Cabanis, E.A., 2007. Cortical projection to the human red nucleus: Complementary results with probabilistic tractography at 3 T. *Neuroradiology* 49 (9), 777–784.
- Horn, A., et al., 2017. Connectivity Predicts deep brain stimulation outcome in Parkinson disease. *Ann. Neurol.* 82, 67–78.
- Horn, A., Kühn, A.A., 2015. Lead-DBS: A toolbox for deep brain stimulation electrode localizations and visualizations. *Neuroimage* 107, 127–135.
- Jenkinson, M., Bannister, P., Brady, M., Smith, S., 2002. Improved optimization for the robust and accurate linear registration and motion correction of brain images. *Neuroimage* 17 (2), 825–841.
- Jenkinson, M., Smith, S., 2001. A global optimisation method for robust affine registration of brain images. *Med. Image Anal.* 5, 143–156.
- Louis, E.D., Machado, D.G., 2015. Tremor-related quality of life: A comparison of essential tremor vs. Parkinson's disease patients. *Park. Relat. Disord.* 21, 729–735.
- Louis, E.D., Ottman, R., 2014. How many people in the USA have essential tremor? Deriving a population estimate based on epidemiological data. *Tremor Other Hyperkinet. Mov. (N. Y)* 4, 259.
- Lundervold, D.A., Ament, P.A., Holt, P., 2013. Social Anxiety, Tremor Severity, and Tremor Disability: A Search for Clinically Relevant Measures. *Psychiatry J.* 2013, 1–5.
- Meng, F.G., et al., 2013. Deep brain stimulation of the subthalamic nucleus for essential tremor. *Chin. Med. J. (Engl)* 126, 395–396.
- Middlebrooks, E.H., et al., 2018. Structural connectivity-based segmentation of the thalamus and prediction of tremor improvement following thalamic deep brain stimulation of the ventral intermediate nucleus. *NeuroImage Clin.* 20, 1266–1273.
- Middlebrooks, E.H., et al., 2020. Neuroimaging advances in deep brain stimulation: Review of indications, anatomy, and brain connectomics. *Am. J. Neuroradiol.* 41, 1558–1568.
- Papavassiliou, E. et al. Thalamic Deep Brain Stimulation for Essential Tremor: Relation of Lead Location to Outcome. *Neurosurgery* 54, 1120–1130 (2004).
- Park, S.H., Goo, J.M., Jo, C.-H., 2004. Receiver operating characteristic (ROC) curve: Practical review for radiologists. *Kor. J. Radiol.* 5 (1), 11. <https://doi.org/10.3348/kjr.2004.5.1.11>.
- Petersen, M.V., et al., 2017. Probabilistic versus deterministic tractography for delineation of the cortico-subthalamic hyperdirect pathway in patients with Parkinson disease selected for deep brain stimulation. *J. Neurosurg.* 126, 1657–1668.
- Pouratian, N., et al., 2011. Multi-institutional evaluation of deep brain stimulation targeting using probabilistic connectivity-based thalamic segmentation: Clinical article. *J. Neurosurg.* 115, 995–1004.
- Sharifi, S., Nederveen, A.J., Booi, J., van, A.-F., Rootselaar, 2014. Neuroimaging essentials in essential tremor: A systematic review. *NeuroImage: Clinical* 5, 217–231.
- Smith, S.M., 2002. Fast robust automated brain extraction. *Hum. Brain Mapp.* 17 (3), 143–155.
- Tsolaki, E., Downes, A., Speier, W., Elias, W.J., Pouratian, N., 2018. The potential value of probabilistic tractography-based for MR-guided focused ultrasound thalamotomy for essential tremor. *NeuroImage Clin.* 17, 1019–1027.
- Tsolaki, E., Narr, K.L., Espinoza, R., Wade, B., Hellemann, G., Kubicki, A., Vasavada, M., Njau, S., Pouratian, N., 2021. Subcallosal Cingulate Structural Connectivity Differs in Responders and Nonresponders to Electroconvulsive Therapy. *Biol. Psychiatry Cogn. Neurosci. Neuroimaging* 6 (1), 10–19. <https://doi.org/10.1016/j.bpsc.2020.05.010>.
- Yamada, K., et al., 2010. MR imaging of ventral thalamic nuclei. *Am. J. Neuroradiol.* 31, 732–735.